Chem

CellPress

Article

Integration of Pd nanoparticles with engineered pore walls in MOFs for enhanced catalysis

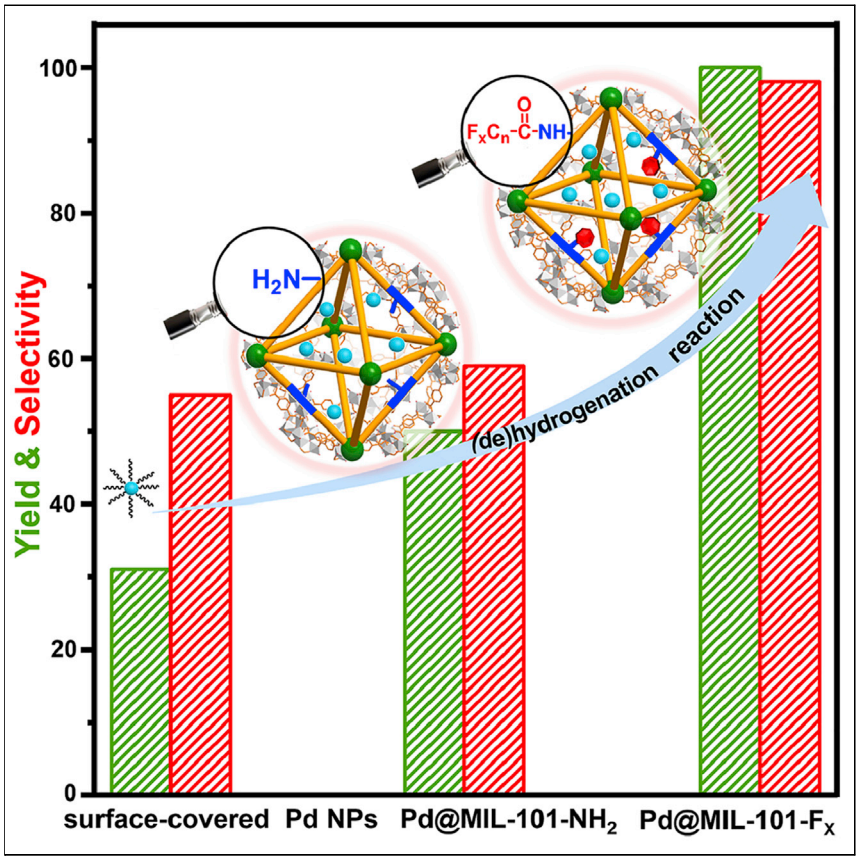

Achieving free-access metal sites with the ability to regulate interactions with substrates is highly desired yet remains a grand challenge in catalysis. Herein, naked Pd nanoparticles were encapsulated inside a metal-organic framework (MOF), giving Pd@MIL-101-NH_2. Its activity and selectivity toward de/hydrogenation reactions can be greatly promoted via the MOF pore wall engineering to regulate Pd surrounding microenvironment and substrate adsorption behavior.

Luyan Li, Zhixin Li, Weijie Yang, ..., Junling Lu, Shu-Hong Yu, Hai-Long Jiang

jianglab@ustc.edu.cn

HIGHLIGHTS

Tunable interaction between metal nanoparticles with substrates is desired

Metal@MOF composites integrate metal nanoparticles with tunable interaction

Tunable microenvironment achieved by metal@MOF via the MOF wettability modification

Enhanced activity/selectivity by modulated microenvironment and substrate enrichment

Li et al., Chem 7, 686–698
March 11, 2021
https://doi.org/10.1016/j.chempr.2020.11.023

CellPress

Chem

Article

Integration of Pd nanoparticles with engineered pore walls in MOFs for enhanced catalysis

Luyan Li,[1] Zhixin Li,[1] Weijie Yang,[2] Yamin Huang,[3] Gang Huang,[1] Qiaoqiao Guan,[1] Yemin Dong,[3] Junling Lu,[1] Shu-Hong Yu,[1] and Hai-Long Jiang[1,4,*]

SUMMARY

Creating free-access active sites and regulating their interaction with substrates are crucial for efficient catalysis, yet remain a grand challenge. Herein, naked Pd nanoparticles (NPs) have been encapsulated in a metal-organic framework (MOF), MIL-101-NH_2, to afford Pd@MIL-101-NH_2. The hydrophobic perfluoroalkyls were post-synthetically modified onto -NH_2 group to yield Pd@MIL-101-F_x (x = 3, 5, 7, 11, 15), which engineer the MOF pore walls to regulate Pd surrounding microenvironment and interaction with substrates. As a result, both the dehydrogenation coupling of organosilane and hydrogenation of halogenated nitrobenzenes show that their activity and selectivity can be greatly promoted upon hydrophobic modification due to the favorable substrate enrichment and regulated interactions between Pd and the modified MOF hosts, far surpassing the traditional supported or surfactant-protected Pd NPs. We envision metal NPs@MOF composites would be an ideal platform integrating the inherent activity of well-accessible metal sites with engineered microenvironment via readily tunable MOFs.

INTRODUCTION

Catalysis is closely related to ubiquitous industrial and environmental applications in our daily life. The essence to achieve high-performance catalysis lies in the development of ideal catalysts. Metal nanoparticles (NPs) have been demonstrated to be a class of important heterogeneous catalysts for a wide scope of reactions.[1–4] The regulation of the interaction between substrates and metal NPs has been recognized to play a central role in catalytic efficiency and selectivity. The surface property modulation of metal NPs requires the modification of diverse functional molecules on their surface, which, unfortunately, is unfavorable to the accessibility of active metal sites and, thus, detrimental to activity.[5–7] Therefore, it would be a great target, but it remains a grand challenge to achieve the desired catalysts, which not only feature well-accessible metal NP active sites but also possess tunable interactions between active metal sites and catalytic substrates. Creating hydrophobic microenvironment around metal NPs is highly desirable to afford special affinity to a variety of hydrophobic substrates for improving activity and/or selectivity. Particularly, metal nanoparticulate catalysts with the hydrophobic surface have shown promoted catalytic performance toward dehydrogenation and hydrogenation reactions, which are common and important in the industry.[8–13] In this context, it is expected to achieve two targets: a hydrophobic environment around metal sites and well-accessible metal NPs (as active sites) for excellent catalytic performance. To meet this challenge, it might be an effective solution to isolate surface property modulation of catalysts

The bigger picture

Regulating the interaction between active sites and substrates is of great importance in catalysis. The common strategy is to modify the surface of active sites (mostly, metal nanoparticles/NPs in heterogeneous catalysts) with diverse molecules, which, unfortunately, is unfavorable to substrate accessibility and, thus, detrimental to activity. Therefore, it is highly desired to develop heterogeneous catalysts featuring naked metal NPs, which are simultaneously able to regulate interaction with substrates. This puts forward long-standing contradictory challenges on metal NP-based catalysts: (1) exposed active sites, requiring naked metal surface, for their good accessibility; (2) functional molecules around active sites, affording tunable interaction with substrates, for enhanced activity and selectivity. To meet the above challenges, we judiciously encapsulate surface-naked metal NPs into MOFs, achieving tunable interaction with substrates by engineering the MOF pore wall microenvironment.

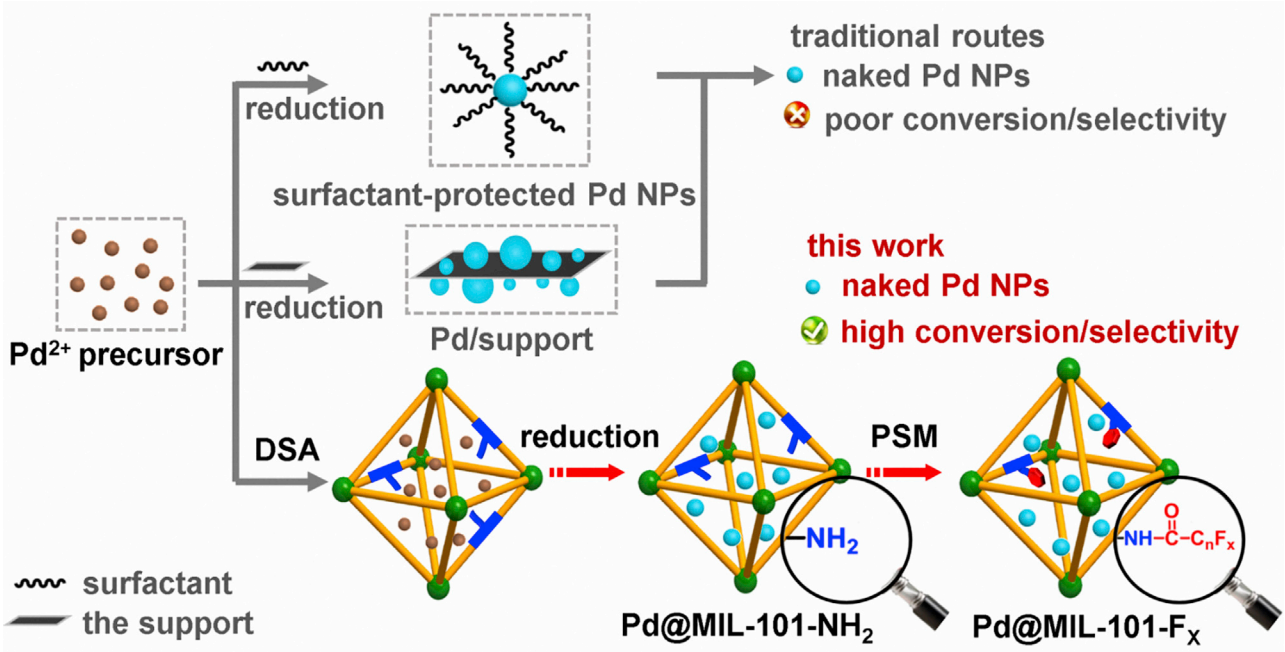

Figure 1. Schematic illustration

Schematic illustration showing (top) the traditional synthesis of the surfactant-protected and support-stabilized Pd NPs and (below) the three steps of the preparation process for Pd@MIL-101-F_x in this work.

from active sites (i.e., metal NPs). The porous hosts incorporating metal NPs are considered to be excellent candidates to achieve the above two targets simultaneously: porous materials encapsulate and stabilize naked metal NPs; whereas, the pore walls can be modified with various functional groups to provide tunable interactions. To this end, a promising class of crystalline porous materials, metal-organic frameworks (MOFs),[14–20] the structures of which are well defined and can be readily tailored at the atomic level, would be ideal hosts for metal NPs. It is worth noting that, although metal NPs stabilized by MOFs have been intensively investigated for catalysis in recent years,[21–35] the chemical environment modulation of MOF pore walls to tailor the catalytic performance of encapsulated metal NPs was rarely explored.[29–35] The limited reports have indicated that the functional groups dangling on the linkers or the metal substitution on the metal-oxo clusters in MOFs are able to significantly affect the electronic properties of exposed metal NPs and/or interaction with reactants, producing enhanced catalytic activity and selectivity.[9,29–35] However, to our knowledge, there has never been a systematic modulation of the wettability environment of MOF pore walls, via simple organic linker modification, to regulate the interaction between the guest metal NPs and substrates for enhanced catalysis.

Bearing the above considerations in mind, a representative mesoporous MOF, MIL-101-NH_2, was employed to encapsulate Pd NPs via the double-solvent method, affording Pd@MIL-101-NH_2 composite. The reactive amino group makes it possible to modulate the chemical environment of MOF pores from hydrophilic –NH_2 to hydrophobic perfluoroalkyl groups by post-synthetic modification (PSM) (Figure 1). The MOF crystallity, Pd sizes, and the accessibility of naked Pd sites remain well after the hydrophobic modification for the MOF. Remarkably, such hydrophobic decoration of pore walls around active Pd NPs significantly boosts the activity toward the dehydrogenation coupling of the organosilane. Moreover, the hydrophobic

[1]Hefei National Laboratory for Physical Sciences at the Microscale, CAS Key Laboratory of Soft Matter Chemistry, College, of Chemistry and Materials Science, University of Science and Technology of China, Hefei, Anhui 230026, China

[2]Department of Power Engineering, School of Energy, Power and Mechanical Engineering, North China Electric Power University, Baoding 071003, China

[3]State Key Laboratory of Functional Materials for Informatics, Shanghai Institute of Microsystem and Information Technology, Chinese Academy of Sciences, Shanghai 200050, China

[4]Lead Contact

*Correspondence: jianglab@ustc.edu.cn

https://doi.org/10.1016/j.chempr.2020.11.023

modification regulates the Pd electronic structure, thereby improving activity and chemoselectivity in the hydrogenation of halogenated nitrobenzenes. It is worth noting that, although there have been a lot of reports on hydrophobic modification of metal NPs, electronic structure regulation of metal catalysts by hydrophobic environment engineering remains extremely rare.

RESULTS AND DISCUSSION

The fabrication of Pd@MIL-101-NH_2 and Pd@MIL-101-F_x

The MIL-101-NH_2, obtained by functionalization of nitro-groups and subsequent reduction to amino for MIL-101, formulated $Cr_3X(H_2O)_2O(BDC)_3$ (X = F or OH, BDC = benzene-1,4-dicarboxylate),[36,37] was employed to incorporate tiny metal NPs. MIL-101-NH_2 features a 3D mesoporous network with ~3 nm cages, high stability, as well as large surface area, suitable for hosting metal NPs. To prevent metal NPs from depositing on the MOF surface, a double-solvent approach (DSA) was adopted to introduce Pd^{2+} aqueous solution into the MOF cages,[38,39] followed by reducing Pd^{2+} by ammonia borane to afford Pd@MIL-101-NH_2. Subsequently, the perfluoroalkyl anhydride or carboxylic acids, $C_nF_{2n+1}CO$-R (n = 1, 2, 3, R = –$OOCC_nF_{2n+1}$; n = 5, 7, R = –OH), were grafted onto the pore walls of Pd@MIL-101-NH_2 via post-synthetic modification (PSM) based on the reaction between –NH_2 and –CO-R groups,[40–42] yielding the products simply denoted as Pd@MIL-101-F_x (Figure S1).

Characterizations of Pd@MIL-101-NH_2 and Pd@MIL-101-F_x

Powder X-ray diffraction (XRD) profiles suggest that the MOF structure is maintained well during the preparation of Pd@MIL-101-NH_2 and subsequent perfluoroalkyl modification (Figure 2A). The absence of identifiable Pd diffraction peak indicates the possibly low Pd content and/or small Pd sizes. Nitrogen sorption results at 77 K suggest that, in reference to Pd@MIL-101-NH_2 (1,849 m^2/g), Brunauer-Emmett-Teller (BET) surface area of the derived Pd@MIL-101-F_x presents an apparent decrease to 600–1,500 m^2/g, due to the pore space occupation by different lengths of perfluoroalkyl chains (Figure S2A). Pore size distribution indicates that the pore space in the MOF is partly occupied by the introduced perfluoroalkyl chains (Figure S2B). Moreover, the elemental mapping result clearly shows that the introduced perfluoroalkyl chains are well distributed throughout the Pd@MIL-101-F_{15} (Figure S3).

The decoration of the hydrophobic perfluoroalkyl groups was probed by Fourier-transform infrared (FTIR) spectroscopy. Compared to Pd@MIL-101-NH_2, two emerged peaks at 1,665 and 1,219 cm^{-1} are, respectively, corresponding to the C=O and C-N bonds of an amide unit in Pd@MIL-101-F_x (Figure S4). The results are supported by X-ray photoelectron spectroscopy (XPS) data. The peak of Pd $3d_{5/2}$ (335.7 eV)[43] presents an apparent shift to ~336 eV in Pd@MIL-101-F_x after modifying the electron-withdrawing perfluoroalkyl groups, implying their successful introduction and the electron transfer from Pd to modified MOF (Figure S5A). The new N 1s peak around 400.8 eV appears in the hydrophobic Pd@MIL-101-F_x (x = 3, 5, 15) due to the formation of the amide unit (Figure S5B).[44] The linker modification can be further supported by digested Pd@MIL-101-F_x samples by ^{19}F NMR with a similar modification ratio (Figure S6). The Pd content in Pd@MIL-101-NH_2 is 1.1 wt %, which is slightly decreased to ~0.7–1.0 wt % in Pd@MIL-101-F_x (Table S1), probably due to the increased weight of introduced groups and/or slight Pd leaching during the modification, while the sizes of Pd NPs (0.8~2 nm) are well retained (Figures 2B, 2C, and S7). The water contact angle of Pd@MIL-101-NH_2 is ~5°, which significantly increases from 50° to 150° along with introducing longer perfluoroalkyl chains (Figure 2D), clearly demonstrating that the modification enables Pd@MIL-101-F_x very hydrophobic. The hydrophobic behavior of Pd@MIL-101-F_x is also supported

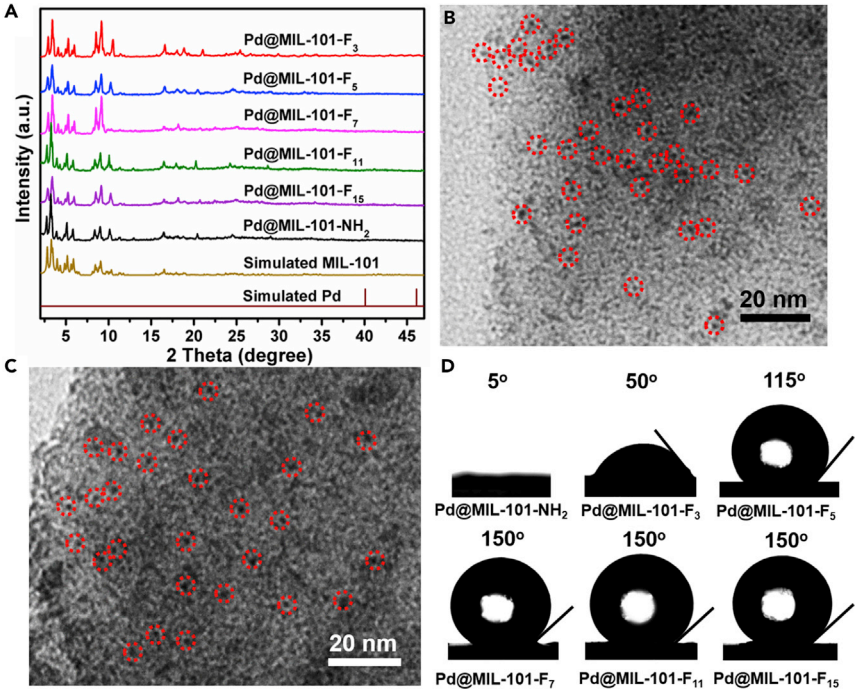

Figure 2. Powder XRD patterns, TEM images, and Static water contact angles

(A–C) (A) Powder X-ray diffraction (XRD) patterns for experimental Pd@MIL-101-NH_2 and Pd@MIL-101-F_x (x = 3, 5, 7, 11, 15), and simulated MIL-101 and Pd. TEM images of (B) Pd@MIL-101-NH_2 and (C) Pd@MIL-101-F_3 as a representative, where the tiny Pd NPs are marked with red circles (scale bar, 20 nm).

(D) Static water contact angles of Pd@MIL-101-NH_2 and Pd@MIL-101-F_x (x = 3, 5, 7, 11, 15).

by the decreased water vapor adsorption with the increased length of perfluoroalkyl chains (Figure S8). Remarkably, the facts of Pd NPs located inside the MOFs before and after perfluoroalkyl modification have been unambiguously verified by taking Pd@MIL-101-NH_2 and Pd@MIL-101-F_3 as representatives, based on the high-angle annular dark-field scanning transmission electron microscopy (HAADF-STEM) tomography and 3D reconstruction results (Figures 3 and S9; see Videos S1 and S2).

The determination of accessible Pd sites in Pd@MIL-101-NH_2 and Pd@MIL-101-F_x

To determine the available active Pd sites before and after the post-synthetic modification, the CO titration experiments for Pd@MIL-101-NH_2, Pd@MIL-101-F_3, and Pd@MIL-101-F_{15} have been carried out. As expected, the Pd@MIL-101-NH_2 and Pd @MIL-101-F_3 have Pd dispersion of ~50%, corresponding to approximately 2 nm particle diameters, which are comparable to the data (0.8~2 nm) from TEM observation indicated above (Table S2). The results indicate that the Pd sites inside the MOF are well accessible, and the number of available Pd sites does remain well before and after the hydrophobic modification in our catalysts. It is worth noting that the Pd dispersion (~40%) of Pd@MIL-101-F_{15} presents a slight decrease even after grafting the very long perfluoroalkyl chains, where the dispersion is still larger than that of the Pd/Al_2O_3-PVP (~5%) because of the blocking of Pd surface by PVP.

Catalytic performance investigation on the dehydrogenation coupling of triethylsilane with H_2O

It is envisioned that such hydrophobic modification of MOF pore walls around Pd NPs would significantly promote the performance toward catalytic dehydrogenation

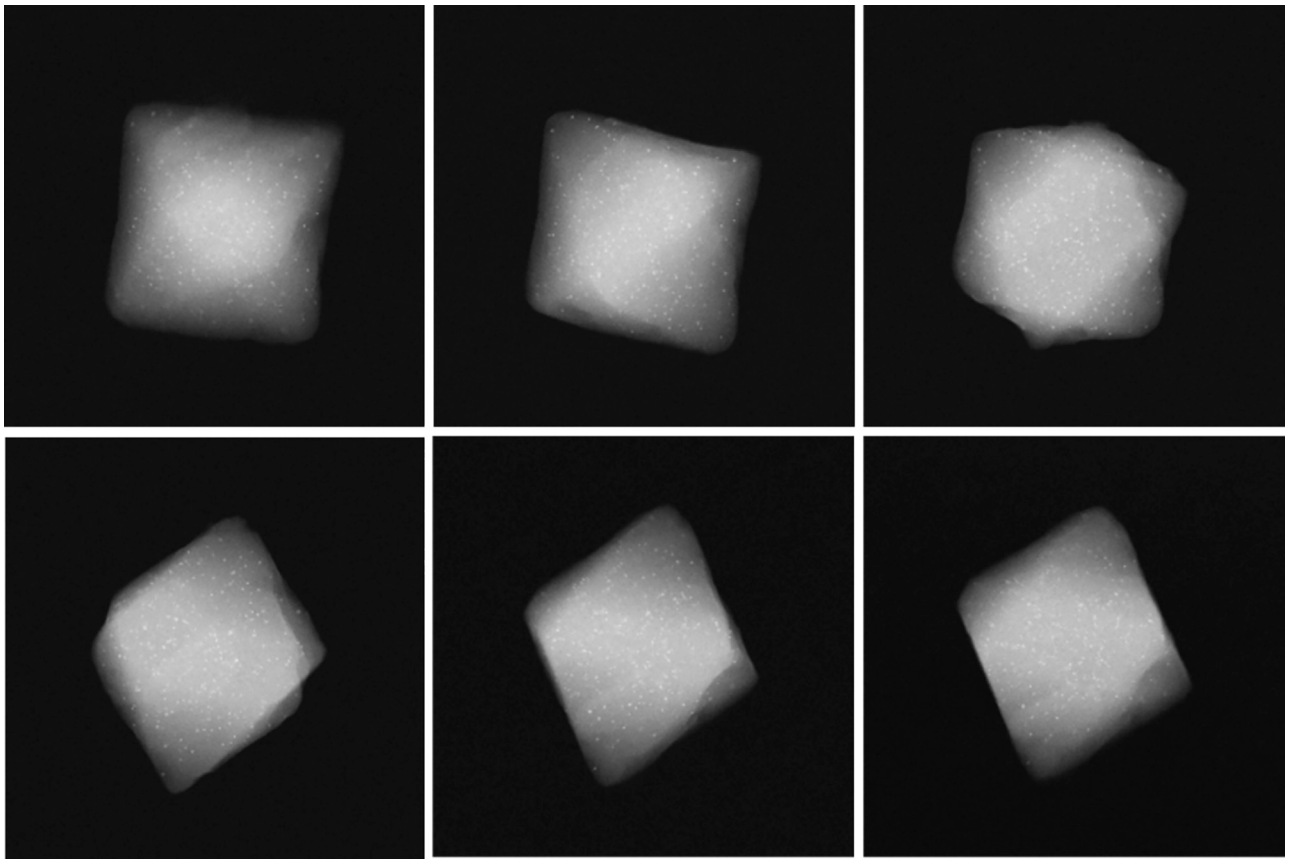

Figure 3. HAADF-STEM images

The representative HAADF-STEM images captured from the video with a series of tilting angles for Pd@MIL-101-F_3 sample taken with 2° tilt increment step from 58° to −56°. The images (from left to right, top to down) are captured at 58°, 56°, 30°, 4°, −22°, and −56°, respectively.

and hydrogenation reactions, which are usually based on Pd catalysts. The dehydrogenative cross-coupling (DCC) reactions between organosilanes and water or alcohols are promising to precisely construct new Si–O bonds via direct Si–H activation.[8,45] The dehydrogenation of triethylsilane with H_2O to triethylsilanol was then investigated. The Pd@MIL-101-NH_2 gave only 50% conversion (Table 1, entry 1). By grafting a short perfluoroalkyl (F_3) group, the conversion was slightly improved to 58% (Table 1, entry 2). Strikingly, the value was elevated to 100% with Pd@MIL-101-F_5 and its turnover frequency (TOF_{Pd}) is 1.2 times higher than Pd@MIL-101-NH_2 (Table 1, entry 3). Along with further increased chain length, the conversion inversely decreases, possibly due to the pore size limit and mass transfer hindrance (Table 1, entries 4–6). The results indicate that hydrophobic environment around Pd NPs does greatly enhance the catalytic efficiency, while too long hydrophobic chains might impair the accessibility of Pd active sites. Almost no conversion can be observed over MIL-101-F_3, indicating that both MIL-101-NH_2 and the modified perfluoroalkyl chains are inactive but Pd NPs are the real active sites (Table 1, entry 7). As controls, Pd NPs supported on Al_2O_3 and Fe_2O_3 were also synthesized and, respectively, showed 38% and 35% conversions (Table 1, entries 8–9), lower than Pd@MIL-101-NH_2 and Pd@MIL-101-F_x, probably due to the enrichment effect of triethylsilane in MOFs. Despite the conversion displayed a slight increase with the Pd/C catalyst (56%), it is much lower than Pd@MIL-101-F_5 (Table 1, entry 10). Moreover, Pd/Al_2O_3 modified with

Table 1. Dehydrogenation coupling of triethylsilane with H_2O over different catalysts

$Et_3Si-H(1a)+H_2O \rightarrow Et_3Si-OH+H_2+$ others

Entry[a]	Cat.	Time (min)	Yield (%)[d]	TOF_{Pd} (min^{-1})
1	Pd@MIL-101-NH_2	5	50	87.1
2	Pd@MIL-101-F_3	5	58	127.7
3	Pd@MIL-101-F_5	5	>99	191.6
4	Pd@MIL-101-F_7	5	79	189.2
5	Pd@MIL-101-F_{11}	5	61	146.1
6	Pd@MIL-101-F_{15}	5	44	120.4
7	MIL-101-F_3	5	–	–
8[b]	Pd/Al_2O_3	5	38	80.9
9[b]	Pd/Fe_2O_3	5	35	74.5
10[b]	Pd/C	5	56	119.1
11[b]	Pd/Al_2O_3-PVP	5	31	66.0
12[c]	Pd/Al_2O_3-F_3	5	40	95.8
13[c]	Pd/Al_2O_3-F_5	5	42	100.6

[a]Reaction conditions: 0.9 mmol **1a**, 10 mg cat., 0.5 mL H_2O, 10 mL THF, air atmosphere, 25°C.
[b]Pd content: 0.9 wt %.
[c]Pd content: 0.8 wt %.
[d]Catalytic reaction products were analyzed and identified by gas chromatography.

surfactant PVP gave only 31% conversion (Table 1, entry 11). Upon modifying perfluoroalkyl chains onto the Pd/Al_2O_3 surface, the conversion was slightly improved to 40% or 42% (Table 1, entries 12–13). The solvent effect in this reaction can be excluded (Table S3). These results clearly show that the created hydrophobic environment around Pd NPs, via MOF modification, gives much superior activity to the traditional Pd catalysts with or without further modification.

The triethylsilane liquid-phase adsorption over Pd@MIL-101-NH_2 and Pd@MIL-101-F_x

To get insight into the improved activity, triethylsilane adsorption experiments have been investigated (Figure S10). Apparently, the resulting Pd@MIL-101-F_x are more favorable to the enrichment and adsorption of hydrophobic triethylsilane than Pd@MIL-101-NH_2. Among all adsorbents investigated, Pd@MIL-101-F_5 possesses optimal adsorption rate while Pd@MIL-101-F_x with decreased or increased F numbers present lower rates, following the same order with the catalytic activity (Figure S11). These results unambiguously suggest that the hydrophobic MOF pore environment enables efficient accumulation of hydrophobic substrate (triethylsilane) and facilitates its enrichment around Pd active sites, thereby accelerating conversion. Moreover, the MOF protects Pd NPs from aggregation, thus the structure and activity of Pd@MIL-101-F_5 can be well maintained after 3 runs (Figures S12 and S13).

Activity investigation on dehydrogenation coupling of various organosilanes with H_2O

Upon optimization of reaction conditions using triethylsilane as a probe substrate, various organosilanes have been examined over Pd@MIL-101-F_5. Not surprisingly, irrespective of replacing the ethyl with electron-donating (-CH_3, -*i*Pr) or withdrawing (-OEt) group, the conversion can be completed in an efficient way, suggesting the advantage and power of the hydrophobically modified catalyst (Table S4).

Catalytic performance investigation on the selective hydrogenation of *p*-nitrochlorobenzene

Encouraged by the outstanding catalytic performance of Pd NPs promoted by creating a hydrophobic pore environment in the MOF, the Pd@MOF catalysts

Table 2. Selective hydrogenation of *p*-nitrochlorobenzene over different catalysts

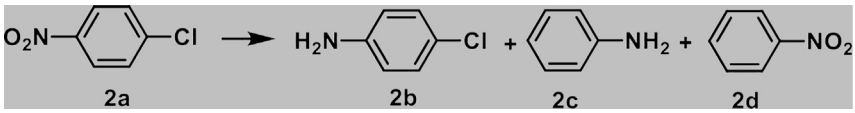

				Yield (%)[i]			
Entry[a]	Cat.	Con. (%)	Sel. to 2b (%)	2b	2c	2d	TOF_{Pd} (min^{-1})
1	Pd@MIL-101-NH_2	>99	59	59	41	–	2.9
2	Pd@MIL-101-F_3	>99	98	98	2	–	6.1
3	Pd@MIL-101-F_5	95	95	90	5	–	5.0
4	Pd@MIL-101-F_7	68	97	66	2	–	4.5
5	Pd@MIL-101-F_{11}	40	97	38	2	–	3.0
6	Pd@MIL-101-F_{15}	20	98	19	1	–	1.5
7[b]	Pd@MIL-101-F_3	91	98	89	2	–	9.1
8[c]	Pd@MIL-101-F_5	90	95	86	4	–	6.1
9[d]	Pd@MIL-101-F_7	92	96	88	4	–	3.9
10[e]	Pd@MIL-101-F_{11}	91	94	86	8	–	1.5
11[e]	Pd@MIL-101-F_{15}	90	94	86	8	–	1.5
12	MIL-101-F_3	<1	–	–	–	–	–
13[f]	Pd@MIL-101	93	40	37	56	–	0.8
14[f]	Pd@MIL-101(F3)	90	81	73	17	–	1.5
15[g]	Pd/Al_2O_3	47	59	28	19	–	1.7
16[g]	Pd/Fe_2O_3	45	54	24	21	–	1.5
17[g]	Pd/C	49	60	29	20	–	1.8
18[g]	Pd/Al_2O_3-PVP	40	55	22	18	–	1.3
19[h]	Pd/Al_2O_3-F_3	50	69	34.5	15.5	–	2.4
20[h]	Pd/Al_2O_3-F_5	48	60	29	19	–	2.0

[a]Reaction conditions: 0.2 mmol **2a**, cat. 15 mg, 3.5 mL toluene, H_2 atmosphere, 8 bar, 90°C, 26 min.
[b]16 min.
[c]20 min.
[d]40 min.
[e]120 min.
[f]Pd content: 0.7 wt%, 100 min.
[g]Pd content: 0.9 wt%.
[h]Pd content: 0.8 wt%.
[i]Catalytic reaction products were analyzed and identified by gas chromatography.

have been further employed for hydrogenation reactions. Selective hydrogenation of *p*-nitrochlorobenzene (**2a**) to *p*-chloroaniline (**2b**), an important chemical intermediate in fine chemistry,[46–49] was investigated. Typically, the dechlorination process of Pd@MIL-101-NH_2 led to only 59% selectivity to **2b** (Table 2, entry 1). Strikingly, the Pd@MIL-101-F_3 showed complete conversion and 98% selectivity to **2b** and the selectivity could be maintained for a prolonged time (Table 2, entry 2, and Figure S14). With the increased length of perfluoroalkyl chain, the activity significantly decreased (Table 2, entries 3–6); they gave similar selectivity at the same conversion (Table 2, entries 7–11). The optimal catalyst, Pd@MIL-101-F_3, toward this reaction is not the same as that in the previous dehydrogenation of triethylsilane, which is probably due to the slight hydrophobic difference of the reaction substrates. The results indicated that the hydrophobic modification favors the reduction of the -NO_2 group over dechlorination in the selective hydrogenation of *p*-nitrochlorobenzene. After grafting very long perfluoroalkyl chains, the reduced conversion might be caused by the pore-blocking effect to varying degrees, restricting the accessibility of the substrate to Pd sites. It is assumed that both hydrophobic environment and accessibility of Pd active sites play critical roles in the resulting catalytic performance. In

control experiments, the hydrogenation reaction did not proceed with MIL-101-F_3, revealing that Pd NPs provided active sites (Table 2, entry 12). The significant dechlorination process observed in the reaction over Pd@MIL-101 revealed that the amine group was not responsible for the selectivity (Table 2, entry 13). Moreover, when modifying the alkyl chains on the MOF pore wall, the dechlorination process cannot be avoided with Pd@MIL-101-CH_3 or Pd@MIL-101-C_7H_{15}, indicating that the perfluoroalkyl groups have a better effect on the selectivity than alkyl chains (Table S5). Accordingly, the derivative of Pd@MIL-101 with trifluoroacetic acid modified onto the Cr-oxo clusters, namely Pd@MIL-101(F_3), can promote the selective hydrogenation (Table 2, entry 14), though slightly inferior to Pd@MIL-101-F_3. The results indicate that the modification of either linker or M-oxo cluster in MOFs is effective to regulate the microenvironment of the hosted Pd NPs for enhanced catalysis. The hydrogenation reaction over Pd/Al_2O_3, Pd/Fe_2O_3, or Pd/C was examined and exhibited below 50% conversions, where the TOF_{Pd} of Pd@MIL-101-F_3 is 2.4∼3.1 times higher than these three catalysts (Table 2, entry 1, entries 15–17). The surfactant PVP-modified Pd/Al_2O_3 also gave decreased activity, possibly due to the PVP influence on the transport of the substrates (Table 2, entry 18). After the hydrophobic modification of Pd/Al_2O_3, both activity and selectivity displayed a slight increase (Table 2, entries 19–20), further reflecting the advantage of a hydrophobic environment in promoting catalytic performance. The solvent effect investigation suggests that the improved catalytic performance of the hydrophobic sample is independent of the solvent used in this reaction (Table S6).

The chlorobenzene or nitrobenzene adsorption investigation over different catalysts

To gain insight into the high selectivity achieved with Pd@MIL-101-F_3, diffuse reflectance infrared Fourier transform spectroscopy (DRIFTS) measurements were carried out to examine the adsorption behavior of Pd@MIL-101-NH_2 and Pd@MIL-101-F_3. With chlorobenzene as the probe molecule, the band at 1,475–1,480 cm^{-1} assignable to the C=C bond of benzene[46] was observed for both catalysts (Figure 4A), whereas no apparent signal was be observed with MIL-101-F_3 (Figure S15). The above facts unambiguously indicate that the chlorobenzene chemisorption takes place on the Pd sites but not by the MOF.[46] However, in contrast to the strong adsorption peak of Pd@MIL-101-NH_2, Pd@MIL-101-F_3 displayed a very weak signal. This weak adsorption of chlorobenzene by Pd@MIL-101-F_3 should be detrimental to its dechloridation conversion, which is conversely favorable to the targeted hydrogenation selectivity. The comparable C=C signal of Pd@MIL-101-F_3 and Pd@MIL-101-F_5 (Figure S15), acting as a representative of other counterparts with high F numbers, also explains the similar selectivity toward hydrogenation process. This assumption can be further supported by the competitive adsorption experiments with a mixture of chlorobenzene (CB) and nitrobenzene (NB) (Figure 4B). The bands at 1,350 and 1,530 cm^{-1} are attributed to N=O bond (nitrobenzene) adsorbed onto the surface of Pd NPs, whereas the 1,480 cm^{-1} signal is originated from both N=O and C=C bonds.[46] For Pd@MIL-101-NH_2, the adsorption strength at 1,480 cm^{-1} is evidently stronger than that at 1,350 and 1,530 cm^{-1}, suggesting both CB and NB are easily adsorbed. In contrast, the signal strength at 1,480 cm^{-1} is almost similar to that at 1,350 and 1,530 cm^{-1} for Pd@MIL-101-F_3, and the adsorption strength of the N=O bond (NB) is comparable to that for Pd@MIL-101-NH_2. This result can be further supported by the density functional theory (DFT) calculation, in which the -NO_2 group is preferentially adsorbed on the positively charged Pd in Pd@MIL-101-F_x with a slightly lower adsorption energy (−0.26 eV) than that on the netural Pd surface in the Pd@MIL-101-NH_2 (Figure S16A). Moreover, the negative charge of -NO_2 (−0.238 e) is larger than -Cl (−0.104 e), indicating that compared to the -Cl group, -NO_2 group is also more likely attracted on

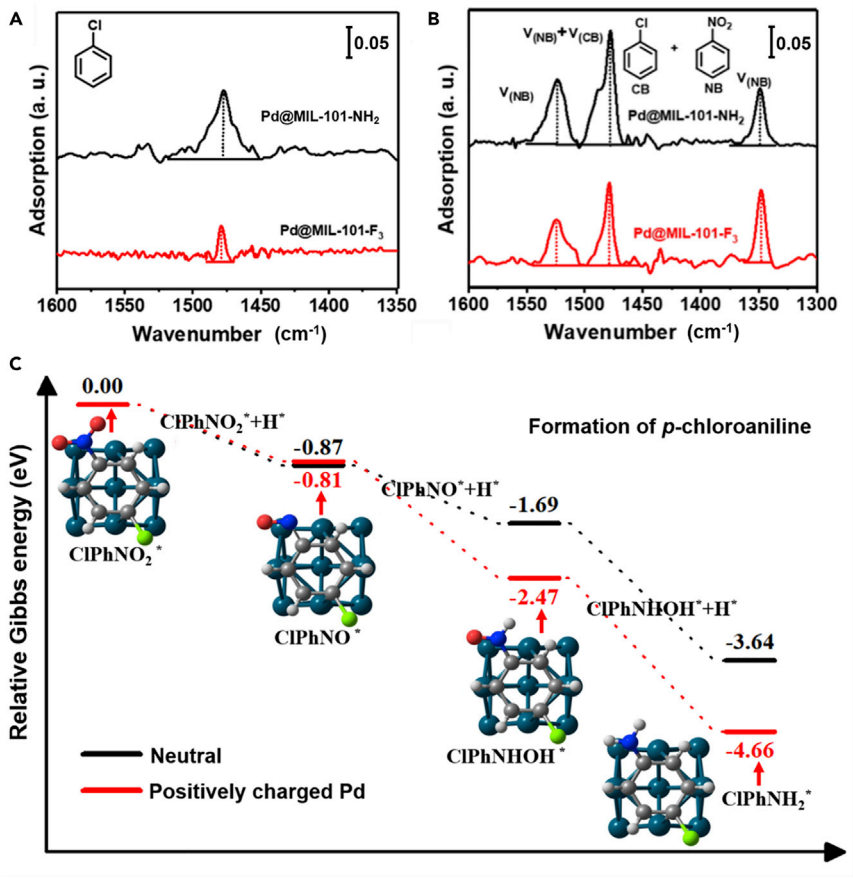

Figure 4. DRIFTS spectra and DFT calculation for the hydrogenation of *p*-nitrochlorobenzene

(A and B) (A) DRIFTS spectra of chlorobenzene or (B) the mixture of chlorobenzene and nitrobenzene adsorbed onto the Pd active sites in Pd@MIL-101-NH_2 and Pd@MIL-101-F_3 (scale bar, 0.05).

(C) Gibbs free energy variation along the reaction coordinate of hydrogenation of *p*-nitrochlorobenzene on netutral or positively charged Pd_{13} cluster. O atom (red); N atom (blue); Cl atom (green); C (gray); and H (white).

the surface of positively charged Pd in Pd@MIL-101-F_3 based on Coulomb's law (Figure S16B). Therefore, it is assumed that the NB tends to be adsorbed on the Pd surface in Pd@MIL-101-F_3, and the CB adsorption is negligible in this hydrophobically modified catalyst. These results demonstrate that the hydrophobic environment created by the MOF modification probably contributes to the preferable adsorption of -NO_2 over -Cl group onto the positively charged Pd active sites in Pd@MIL-101-F_x, leading to the high selectivity of hydrogenation to yield *p*-chloroaniline.

The CO-DRIFTS spectra for Pd@MIL-101-NH_2 and Pd@MIL-101-F_3

The DRIFTS spectra with CO as the probe molecule were collected to confirm the electron interaction between Pd and the MOF (Figure S17). Compared to the Pd@MIL-101-NH_2, the red-shift of the peak to 2,042 cm^{-1} occurs in Pd@MIL-101-F_3, suggesting the strong interaction between Pd and the hydrophobically modified the framework. The results reflect that the electrons are transferred from the Pd surface to the host framework in Pd@MIL-101-F_3, probably resulting in the positively charged Pd surface, which is in good agreement with the peak shift between Pd and hydrophobic host framework in XPS data (Figure S5).

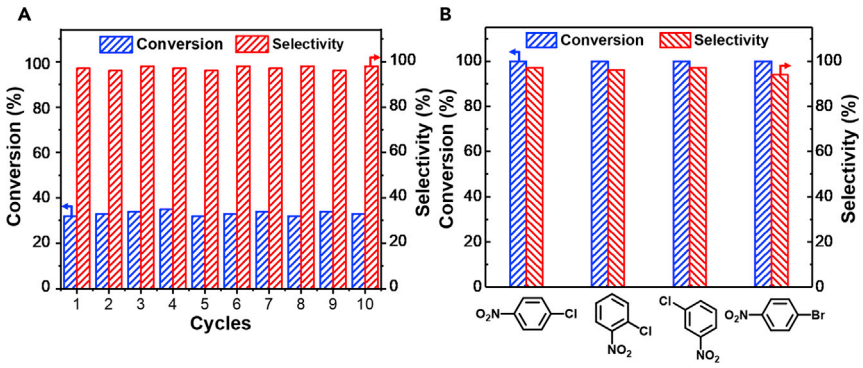

Figure 5. Stability test and the hydrogenation of various halogenated nitrobenzenes

(A) Catalytic conversion and selectivity over Pd@MIL-101-F_3 (8 mg) during the 10 runs for the selective hydrogenation of *p*-nitrochlorobenzene (0.25 mmol).

(B) The hydrogenation of various halogenated nitrobenzenes over Pd@MIL-101-F_3.

The DFT calculation for the hydrogenation of *p*-nitrochlorobenzene

Inspired by the electron transfer based on the XPS and CO-DRIFTS data, the neutral Pd_{13} and positively charged Pd_{13} models have been fabricated to calculate the selective hydrogenation process of *p*-nitrochlorobenzene. In the beginning, the adsorption energy of substrates on the Pd surface had been calculated. The results show that *p*-nitrochlorobenzene tends to be adsorbed on the positively charged Pd surface (Figure S18). Then, to further investigate the reaction mechanism, the Gibbs free energy variation along the reaction coordinate of the two reaction paths (**path I** and **path II**) have been investigated according to the previous work (Figures 4C and S19).[50] Compared to **path II**, **path I** related to the formation of *p*-chloroaniline is thermodynamically favored (Figure S19). In **path I**, the generation of $ClPhNO_2$* and ClPhNO* is a similar exothermic process on both neutral Pd and positively charged Pd surface. Significantly, the ClPhNHOH intermediate is prone to be generated on the positively charged Pd surface with the relative energy of −2.47 eV in **path I** (Figure 4C). Moreover, the hydroxyl dissociation from ClPhNHOH also easily takes place on the positively charged Pd surface, generating the *p*-chloroaniline with the relative energy of −4.66 eV, which is lower than the neutral Pd (−3.64 eV). Thus, the *p*-chloroaniline is preferentially generated on the positively charged Pd sites. The above DFT calculation results clearly suggest that, compared to the neutral Pd in the Pd@MIL-101-NH_2, the positively charged Pd sites in Pd@MIL-101-F_x contribute to the preferable selectivity to *p*-chloroaniline.

Stability and recyclability have been further investigated. Significantly, both catalytic activity and selectivity of Pd@MIL-101-F_3 can be well maintained in the hydrogenation of *p*-nitrochlorobenzene even after 10 consecutive runs (Figure 5A). Importantly, the supernatant fluid after the recycling experiment does not give ^{19}F NMR signal (Figure S20), revealing high stability of the Pd@MIL-101-F_3 catalyst during the process. Moreover, both TEM image and powder XRD pattern of Pd@MIL-101-F_3 are well retained after reaction, indicating that the MOF is robust under these reaction conditions and it prevents Pd NPs from aggregation (Figure S21). The optimal catalyst, Pd@MIL-101-F_3, has also been examined by the hot filtration test. No Pd leaching can be found in the filtrate based on inductively coupled plasma atomic emission spectrometer (ICP-AES) analysis and no further increase in the conversion occurs after removing the solid catalyst (Figure S22), demonstrating its nature of truly heterogeneous catalysis. To explore the scope of substrates, the nitrobenzene functionalized with chloro group at different positions have been

investigated over Pd@MIL-101-F_3 (Figure 5B). Both *o*-nitrochlorobenzene and *m*-nitrochlorobenzene can be conversed to the corresponding chloroaniline completely with 97% selectivity. Moreover, after replacing the -Cl with -Br, *p*-nitrobromobenzene can also be transformed to *p*-bromoaniline with 94% selectivity (Figure 5B). Therefore, the microenvironment around well-accessible Pd NPs endowed by facile MOF hydrophobic modification can not only boost the activity but also cause the selective adsorption to improve the catalytic selectivity.

Conclusion

In summary, by integrating well-accessible Pd NPs and easily functionalizable MOF, we have synthesized Pd@MIL-101-NH_2 and its furnished materials Pd@MIL-101-F_x (x = 3, 5, 7, 11, 15), where perfluoroalkyl groups are grafted onto the MOF pore walls to regulate the hydrophobic environment around Pd sites. The Pd@MIL-101-F_5 exhibits high catalytic activity and recyclability in the dehydrogenation coupling of organosilanes due to the enrichment effect for the hydrophobic substrates. In addition, the highly selective hydrogenation of nitrochlorobenzenes, where the dechlorination process is significantly suppressed, can be effectively promoted with Pd@MIL-101-F_3. The optimized hydrophobic modification of the MOF pore walls creates the interaction with Pd and gives rise to the positively charged Pd surface in Pd@MIL-101-F_x, leading to the favorable adsorption of -NO_2 over -Cl and the highly selective hydrogenation. Furthermore, both catalysts present excellent recyclability due to the MOF protection for Pd NPs against aggregation/leaching. It is acknowledged that the naked Pd NPs facilitate access to substrates, accelerating their conversion; and the engineered MOF pore walls not only benefit the substrate enrichment but also regulate the electronic state of Pd to control the interaction between Pd and substrates, further boosting the activity and dominating the high selectivity. This work, by rationally fabricating a single composite catalyst, would open a new avenue to the integration of well-accessible active sites with their surface microenvironment regulation based on the tailorability of host porous materials for enhanced catalysis.

EXPERIMENTAL PROCEDURES

Resource availability

Lead contact

Further information and requests for resources and reagents should be directed to and will be fulfilled by the Lead Contact, Hai-Long Jiang (jianglab@ustc.edu.cnjianglab@ustc.edu.cn).

Materials availability

The materials generated in this study will be made available on request.

Data and code availability

All data supporting this study are available in the manuscript and Supplemental Information.

SUPPLEMENTAL INFORMATION

Supplemental Information can be found online at https://doi.org/10.1016/j.chempr.2020.11.023.

ACKNOWLEDGMENTS

We are grateful to the editors and the anonymous reviewers for their insightful comments and valuable help and suggestions. This work was supported by the NSFC (21725101, 21871244, 21673213, and 21521001), the Fundamental Research Funds

for the Central Universities (WK2060030029), and Fujian Institute of Innovation (CAS).

AUTHOR CONTRIBUTIONS

H.-L.J. conceived the idea and supervised the project; L.L. performed the experiments and collected the data; Z.L. and G.H. assisted in some experiments; W.Y. conducted and analyzed the DFT calculations; Q.G. and J.L. conducted the DRIFTS experiments; Y.H. and Y.D. worked on the HAADF-STEM tomography and related 3D reconstruction; H.-L.J. and L.L. co-wrote the manuscript and all authors contributed to the overall scientific interpretation and editing of the manuscript.

DECLARATION OF INTERESTS

The authors declare no competing interests.

Received: October 5, 2020
Revised: November 3, 2020
Accepted: November 19, 2020
Published: February 2, 2021

REFERENCES

1. Kattel, S., Ramírez, P.J., Chen, J.G., Rodriguez, J.A., and Liu, P. (2017). Active sites for CO_2 hydrogenation to methanol on Cu/ZnO catalysts. Science *355*, 1296–1299.
2. Liu, L., and Corma, A. (2018). Metal catalysts for heterogeneous catalysis: from single atoms to nanoclusters and nanoparticles. Chem. Rev. *118*, 4981–5079.
3. Kang, H., Buchman, J.T., Rodriguez, R.S., Ring, H.L., He, J., Bantz, K.C., and Haynes, C.L. (2019). Stabilization of silver and gold nanoparticles: preservation and improvement of plasmonic functionalities. Chem. Rev. *119*, 664–699.
4. Vogt, C., Groeneveld, E., Kamsma, G., Nachtegaal, M., Lu, L., Kiely, C.J., Berben, P.H., Meirer, F., and Weckhuysen, B.M. (2018). Unravelling structure sensitivity in CO_2 hydrogenation over nickel. Nat. Catal. *1*, 127–134.
5. Schoenbaum, C.A., Schwartz, D.K., and Medlin, J.W. (2014). Controlling the surface environment of heterogeneous catalysts using self-assembled monolayers. Acc. Chem. Res. *47*, 1438–1445.
6. Wu, B., Huang, H., Yang, J., Zheng, N., and Fu, G. (2012). Selective hydrogenation of α,β-unsaturated aldehydes catalyzed by amine-capped platinum-cobalt nanocrystals. Angew. Chem. Int. Ed. Engl. *51*, 3440–3443.
7. Liu, P., Qin, R., Fu, G., and Zheng, N. (2017). Surface coordination chemistry of metal nanomaterials. J. Am. Chem. Soc. *139*, 2122–2131.
8. Lin, J.-D., Bi, Q.-Y., Tao, L., Jiang, T., Liu, Y.-M., He, H.-Y., Cao, Y., and Wang, Y.-D. (2017). Wettability-driven palladium catalysis for enhanced dehydrogenative coupling of organosilanes. ACS Catal. *7*, 1720–1727.
9. Huang, Y.-B., Shen, M., Wang, X., Huang, P., Chen, R., Lin, Z.-J., and Cao, R. (2016). Water-medium C-H activation over a hydrophobic perfluoroalkane-decorated metal-organic framework platform. J. Catal. *333*, 1–7.
10. Huang, G., Yang, Q., Xu, Q., Yu, S.-H., and Jiang, H.-L. (2016). Polydimethylsiloxane coating for a palladium/MOF composite: highly improved catalytic performance by surface hydrophobization. Angew. Chem. Int. Ed. Engl. *55*, 7379–7383.
11. Meemken, F., and Baiker, A. (2017). Recent progress in heterogeneous asymmetric hydrogenation of C=O and C=C bonds on supported noble metal catalysts. Chem. Rev. *117*, 11522–11569.
12. Marshall, S.T., O'Brien, M., Oetter, B., Corpuz, A., Richards, R.M., Schwartz, D.K., and Medlin, J.W. (2010). Controlled selectivity for palladium catalysts using self-assembled monolayers. Nat. Mater. *9*, 853–858.
13. Aguado, S., Canivet, J., Schuurman, Y., and Farrusseng, D. (2011). Tuning the activity by controlling the wettability of MOF eggshell catalysts: a quantitative structure–activity study. J. Catal. *284*, 207–214.
14. Furukawa, H., Cordova, K.E., O'Keeffe, M., and Yaghi, O.M. (2013). The chemistry and applications of metal-organic frameworks. Science *341*, 1230444.
15. Zhou, H.-C., and Kitagawa, S. (2014). Metal-organic frameworks (MOFs). Chem. Soc. Rev. *43*, 5415–5418.
16. Islamoglu, T., Goswami, S., Li, Z., Howarth, A.J., Farha, O.K., and Hupp, J.T. (2017). Postsynthetic tuning of metal-organic frameworks for targeted applications. Acc. Chem. Res. *50*, 805–813.
17. Li, B., Wen, H.-M., Cui, Y., Zhou, W., Qian, G., and Chen, B. (2016). Emerging multifunctional metal-organic framework materials. Adv. Mater. *28*, 8819–8860.
18. Zhao, X., Wang, Y., Li, D.-S., Bu, X., and Feng, P. (2018). Metal-organic frameworks for separation. Adv. Mater. *30*, e1705189.
19. Chen, L., and Xu, Q. (2019). Metal-organic framework composites for catalysis. Matter *1*, 57–89.
20. Wu, G.-D., Huang, J.-H., Zang, Y., He, J., and Xu, G. (2017). Porous field-effect transistors based on a semiconductive metal-organic framework. J. Am. Chem. Soc. *139*, 1360–1363.
21. Yang, Q., Xu, Q., and Jiang, H.-L. (2017). Metal-organic frameworks meet metal nanoparticles: synergistic effect for enhanced catalysis. Chem. Soc. Rev. *46*, 4774–4808.
22. Lu, G., Li, S., Guo, Z., Farha, O.K., Hauser, B.G., Qi, X., Wang, Y., Wang, X., Han, S., Liu, X., et al. (2012). Imparting functionality to a metal-organic framework material by controlled nanoparticle encapsulation. Nat. Chem. *4*, 310–316.
23. Moon, H.R., Lim, D.-W., and Suh, M.P. (2013). Fabrication of metal nanoparticles in metal-organic frameworks. Chem. Soc. Rev. *42*, 1807–1824.
24. Hu, P., Morabito, J.V., and Tsung, C.-K. (2014). Core–shell catalysts of metal nanoparticle core and metal-organic framework shell. ACS Catal. *4*, 4409–4419.
25. Liu, H., Chang, L., Bai, C., Chen, L., Luque, R., and Li, Y. (2016). Controllable encapsulation of "clean" metal clusters within mofs through kinetic modulation: towards advanced heterogeneous nanocatalysts. Angew. Chem. Int. Ed. Engl. *55*, 5019–5023.
26. Li, G., Zhao, S., Zhang, Y., and Tang, Z. (2018). Metal-organic frameworks encapsulating active nanoparticles as emerging composites for catalysis: recent progress and perspectives. Adv. Mater. *30*, e1800702.

27. Yuan, B., Pan, Y., Li, Y., Yin, B., and Jiang, H. (2010). A highly active heterogeneous palladium catalyst for the Suzuki–Miyaura and Ullmann coupling reactions of aryl chlorides in aqueous media. Angew. Chem. Int. Ed. Engl. *49*, 4054–4058.

28. Hwang, Y.K., Hong, D.-Y., Chang, J.-S., Jhung, S.H., Seo, Y.-K., Kim, J., Vimont, A., Daturi, M., Serre, C., and Férey, G. (2008). Amine grafting on coordinatively unsaturated metal centers of MOFs: consequences for catalysis and metal encapsulation. Angew. Chem. Int. Ed. Engl. *47*, 4144–4148.

29. Choi, K.M., Na, K., Somorjai, G.A., and Yaghi, O.M. (2015). Chemical environment control and enhanced catalytic performance of platinum nanoparticles embedded in nanocrystalline metal-organic frameworks. J. Am. Chem. Soc. *137*, 7810–7816.

30. Li, X., Goh, T.W., Li, L., Xiao, C., Guo, Z., Zeng, X., and Huang, W. (2016). Controlling catalytic properties of Pd nanoclusters through their chemical environment at the atomic level using isoreticular metal-organic frameworks. ACS Catal. *6*, 3461–3468.

31. Zhao, M., Yuan, K., Wang, Y., Li, G., Guo, J., Gu, L., Hu, W., Zhao, H., and Tang, Z. (2016). Metal-organic frameworks as selectivity regulators for hydrogenation reactions. Nature *539*, 76–80.

32. Liu, H., Chang, L., Chen, L., and Li, Y. (2016). Nanocomposites of platinum/metal-organic frameworks coated with metal-organic frameworks with remarkably enhanced chemoselectivity for cinnamaldehyde hydrogenation. ChemCatChem *8*, 946–951.

33. Li, X., Van Zeeland, R.V., Maligal-Ganesh, R.V., Pei, Y., Power, G., Stanley, L., and Huang, W. (2016). Impact of linker engineering on the catalytic activity of metal-organic frameworks containing Pd (II)-bipyridine complexes. ACS Catal. *6*, 6324–6328.

34. Yoshimaru, S., Sadakiyo, M., Staykov, A., Kato, K., and Yamauchi, M. (2017). Modulation of the catalytic activity of Pt nanoparticles through charge-transfer interactions with metal-organic frameworks. Chem. Commun. *53*, 6720–6723.

35. Zhao, Y., Kornienko, N., Liu, Z., Zhu, C., Asahina, S., Kuo, T.-R., Bao, W., Xie, C., Hexemer, A., Terasaki, O., et al. (2015). Mesoscopic constructs of ordered and oriented metal-organic frameworks on plasmonic silver nanocrystals. J. Am. Chem. Soc. *137*, 2199–2202.

36. Férey, G., Mellot-Draznieks, C., Serre, C., Millange, F., Dutour, J., Surblé, S., and Margiolaki, I. (2005). A chromium terephthalate-based solid with unusually large pore volumes and surface area. Science *309*, 2040–2042.

37. Bernt, S., Guillerm, V., Serre, C., and Stock, N. (2011). Direct covalent post-synthetic chemical modification of Cr-MIL-101 using nitrating acid. Chem. Commun. *47*, 2838–2840.

38. Aijaz, A., Karkamkar, A., Choi, Y.J., Tsumori, N., Rönnebro, E., Autrey, T., Shioyama, H., and Xu, Q. (2012). Immobilizing highly catalytically active Pt nanoparticles inside the pores of metal-organic framework: a double solvents approach. J. Am. Chem. Soc. *134*, 13926–13929.

39. Chen, Y.-Z., Zhou, Y.-X., Wang, H., Lu, J., Uchida, T., Xu, Q., Yu, S.-H., and Jiang, H.-L. (2015). Multifunctional PdAg@MIL-101 for one-pot cascade reactions: combination of host-guest cooperation and bimetallic synergy in catalysis. ACS Catal. *5*, 2062–2069.

40. Cohen, S.M. (2017). The postsynthetic renaissance in porous solids. J. Am. Chem. Soc. *139*, 2855–2863.

41. Bonnefoy, J., Legrand, A., Quadrelli, E.A., Canivet, J., and Farrusseng, D. (2015). Enantiopure peptide-functionalized metal-organic frameworks. J. Am. Chem. Soc. *137*, 9409–9416.

42. Ahnfeldt, T., Gunzelmann, D., Loiseau, T., Hirsemann, D., Senker, J., Férey, G., and Stock, N. (2009). Synthesis and modification of a functionalized 3D open-framework structure with MIL-53 topology. Inorg. Chem. *48*, 3057–3064.

43. Pascanu, V., Carson, F., Solano, M.V., Su, J., Zou, X., Johansson, M.J., and Martín-Matute, B. (2016). Selective heterogeneous C-H activation/halogenation reactions catalyzed by Pd@MOF nanocomposites. Chemistry *22*, 3729–3737.

44. Tawil, N., Sacher, E., Boulais, E., Mandeville, R., and Meunier, M. (2013). X-ray photoelectron spectroscopic and transmission electron microscopic characterizations of bacteriophage-nanoparticle complexes for pathogen detection. J. Phys. Chem. C *117*, 20656–20665.

45. Wang, Y., Wan, X.-K., Ren, L., Su, H., Li, G., Malola, S., Lin, S., Tang, Z., Häkkinen, H., Teo, B.K., et al. (2016). Atomically precise alkynyl-protected metal nanoclusters as a model catalyst: observation of promoting effect of surface ligands on catalysis by metal nanoparticles. J. Am. Chem. Soc. *138*, 3278–3281.

46. Zhang, J., Wang, L., Shao, Y., Wang, Y., Gates, B.C., and Xiao, F.-S. (2017). A Pd@zeolite catalyst for nitroarene hydrogenation with high product selectivity by sterically controlled adsorption in the zeolite micropores. Angew. Chem. Int. Ed. Engl. *56*, 9747–9751.

47. Jagadeesh, R.V., Surkus, A.-E., Junge, H., Pohl, M.-M., Radnik, J., Rabeah, J., Huan, H., Schünemann, V., Brückner, A., and Beller, M. (2013). Nanoscale Fe_2O_3-based catalysts for selective hydrogenation of nitroarenes to anilines. Science *342*, 1073–1076.

48. Cárdenas-Lizana, F., Hao, Y., Crespo-Quesada, M., Yuranov, I., Wang, X., Keane, M.A., and Kiwi-Minsker, L. (2013). Selective gas phase hydrogenation of p-chloronitrobenzene over Pd catalysts: role of the support. ACS Catal. *3*, 1386–1396.

49. Jiang, W., Xu, B., Xiang, Z., Liu, X., and Liu, F. (2016). Preparation and reactivity of UV light-reduced Pd/α-Fe_2O_3 catalyst towards the hydrogenation of *o*-chloronitrobenzene. Appl. Catal. A *520*, 65–72.

50. Lyu, J., Wang, J., Lu, C., Ma, L., Zhang, Q., He, X., and Li, X. (2014). Size-dependent halogenated nitrobenzene hydrogenation selectivity of Pd nanoparticles. J. Phys. Chem. C *118*, 2594–2601.